



The effect of zirconium addition on microstructure and properties of ball milled and hot compacted powder of Al–12 wt% Zn–3 wt% Mg–1.5 wt% Cu alloy

Lidia Lityńska-Dobrzyńska*, Jan Dutkiewicz, Wojciech Maziarz, Anna Góral

Institute of Metallurgy and Materials Science Polish Academy of Sciences, 25 Reymonta St., 30-059 Cracow, Poland

ARTICLE INFO

Article history:

Received 2 July 2010

Received in revised form 31 January 2011

Accepted 1 February 2011

Available online 9 March 2011

Keywords:

Al–Zn–Mg–Cu–Zr alloy

Powder metallurgy

Mechanical alloying

Microstructure

TEM

X-ray diffraction

ABSTRACT

Elemental powders of the composition Al–12 wt% Zn–3 wt% Mg–1.5 wt% Cu with addition of 1 and 2 wt% Zr were ball milled in a planetary high-energy ball mill and then hot pressed in vacuum under 600 MPa pressure at 380 °C. The effect of ball milling and hot pressing on the microstructure was investigated by means of X-ray diffraction measurements (XRD), light microscopy, analytical and scanning transmission electron microscopy (TEM). Ball milling for 80 h leads to homogenous, highly deformed microstructure of aluminium solid solution with grain size below 100 nm. In the powder with zirconium addition, some part of the Zr atoms diffused in aluminium up to 0.3 wt% Zr. The remaining was found to form Zr-rich particles identified as face centered cubic (fcc) phase. Good quality samples without pores and cracks obtained by hot pressing composed of grains and subgrains of size below 200 nm. The particles of MgZn₂ phase were identified which were located mainly between compacted particles of milled powder. Hot pressed powder showed Vickers microhardness of about 195 HV (0.2N) and ultimate compression strength in the range 611–658 MPa in the compression test. Addition of zirconium had no influence on the strength of the compacted powders.

© 2011 Elsevier B.V. All rights reserved.

1. Introduction

The 7XXX series (Al–Zn–Mg–Cu) aluminium alloys are widely used in the aircraft industry due to their low density, high strength and good workability [1]. Their strengthening increases with the increasing concentration of major alloying components (Zn and Mg) and is associated with a higher density of fine precipitates of metastable η' -phase. The high solute (about 8 wt% of Zn) alloy designated AA 7055, V96ts-3 or C912 evokes the highest strength aluminium alloys produced by ingot metallurgy and find application as upper wing skin materials in commercial aircraft [2–4]. Although a limit of about 8 wt% Zn is imposed for conventional cast materials because of foundry problems as solute macrosegregation and cracking, higher Zn and Mg content could be achieved by using new production methods, such as powder metallurgy and spray deposition. For example, super high strength Al–Zn–Mg–Cu alloy containing up to 9 wt% of Zn was developed by compaction of atomized powder and its ultimate tensile strength was about 900 MPa [5], while yield strength of about 850 MPa were reach for spray deposited Al–Zn–Mg–Cu alloy with Zn content up to 12 wt% [6].

Aluminium based materials produced by powder metallurgy (PM) processing offer a number of interesting opportunities for high

strength applications. Powder metallurgy enables to fabricate high quality parts close to final dimensions with refined microstructure as compared with these produced by the conventional ingot metallurgy [7,8]. Ball milling applied before the compaction allows obtaining a very fine grain size in the nano-range and the extension of the solid solubility limits of the elements added to the alloy [9]. It results in an improved mechanical and corrosion properties of the compacted products. PM technology provides more homogenous distribution of precipitates and reduces particle size that makes corrosion more uniform [10].

Addition of zirconium can improve the properties of 7XXX series alloys by forming metastable, coherent with the matrix Al₃Zr dispersoids, which stabilized the grain structure and prevent recrystallization [11]. The addition of higher than standard amount of Zr into the Al alloy in order to enhance their advantageous effect on the alloy properties is possible due to application of powder metallurgy technologies. It was shown, that addition of 1 wt% of Zr to Al–9 wt% Zn–3 wt% Mg–1.3 wt% Cu caused the tensile strength increase up to 880 MPa [12].

The aim of the present investigation was to study the effect of ball milling and hot pressing on the microstructure and properties of the alloy with a high zinc and magnesium content Al–12 wt% Zn–3 wt% Mg–1.5 wt% Cu with zirconium addition.

2. Experimental details

The mixtures of elemental powders of aluminium, zinc, magnesium, copper and zirconium were used as starting materials to yield Al–12 wt% Zn–3 wt%

* Corresponding author. Fax: +48 122952804.

E-mail addresses: nmlityns@imim-pan.krakow.pl, li2505@poczta.onet.pl (L. Lityńska-Dobrzyńska).

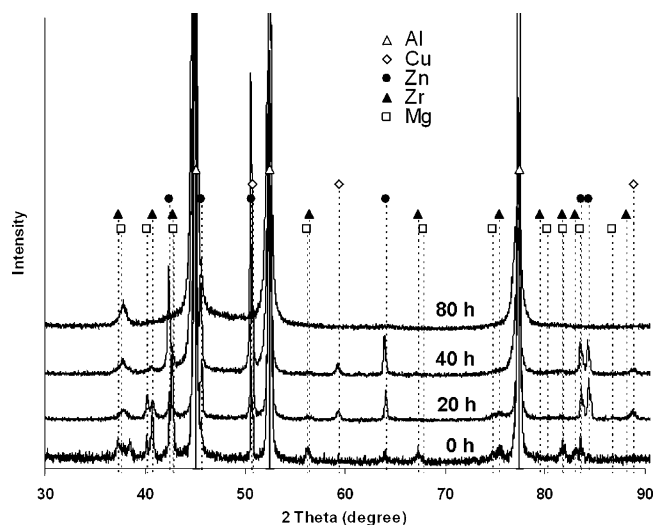


Fig. 1. X-ray diffraction patterns for a sequence of as milled A-2 powder after various milling time.

Mg–1.5 wt% Cu (A-0), Al–12 wt% Zn–3 wt% Mg–1.5 wt% Cu–1 wt% Zr (A-1) and Al–12 wt% Zn–3 wt% Mg–1.5 wt% Cu–2 wt% Zr (A-2) compositions. The ball milling of the powder was performed in a planetary high-energy ball mill Fritsch – P5 in an argon atmosphere using stainless steel balls with diameter 8 mm and a ball to powder weight ratio of 10:1. The ball milled powder was hot pressed in vacuum under 600 MPa pressure at 380 °C for 12 min. The microstructure of the ball milled and compacted powder was investigated by means of X-ray diffraction measurements (XRD) using Philips PW 1710 with CoK α radiation, light microscopy using Leica QWin, analytical transmission electron microscopy (TEM) using FEI Tecnai G² microscope at 200 kV equipped with high-angle annular dark field scanning transmission electron microscopy detector (HAADF-STEM) combined with energy dispersive X-ray (EDX) EDAX microanalysis. The camera length of 200 mm was chosen for the STEM mode, appropriate for Z-contrast HAADF imaging. In order to prepare the TEM samples from the ball milled powder thin slices of the powders embedded in a kit recommended by Leica were cut using Leica EM UC6 ultramicrotome with a diamond knife and then placed on a carbon film supported by a copper grid. A TenuPol-5 double-jet electropolisher was used for the thin-foil preparation from the compacted powder in an electrolyte containing nitric acid and methanol (1:3), at temperature –30 °C and voltage 15 V. Microhardness Vickers measurements were performed using a CSM-Instruments microhardness tester. The Instron testing machine with external measurement of the sample dimensions was used for compression tests.

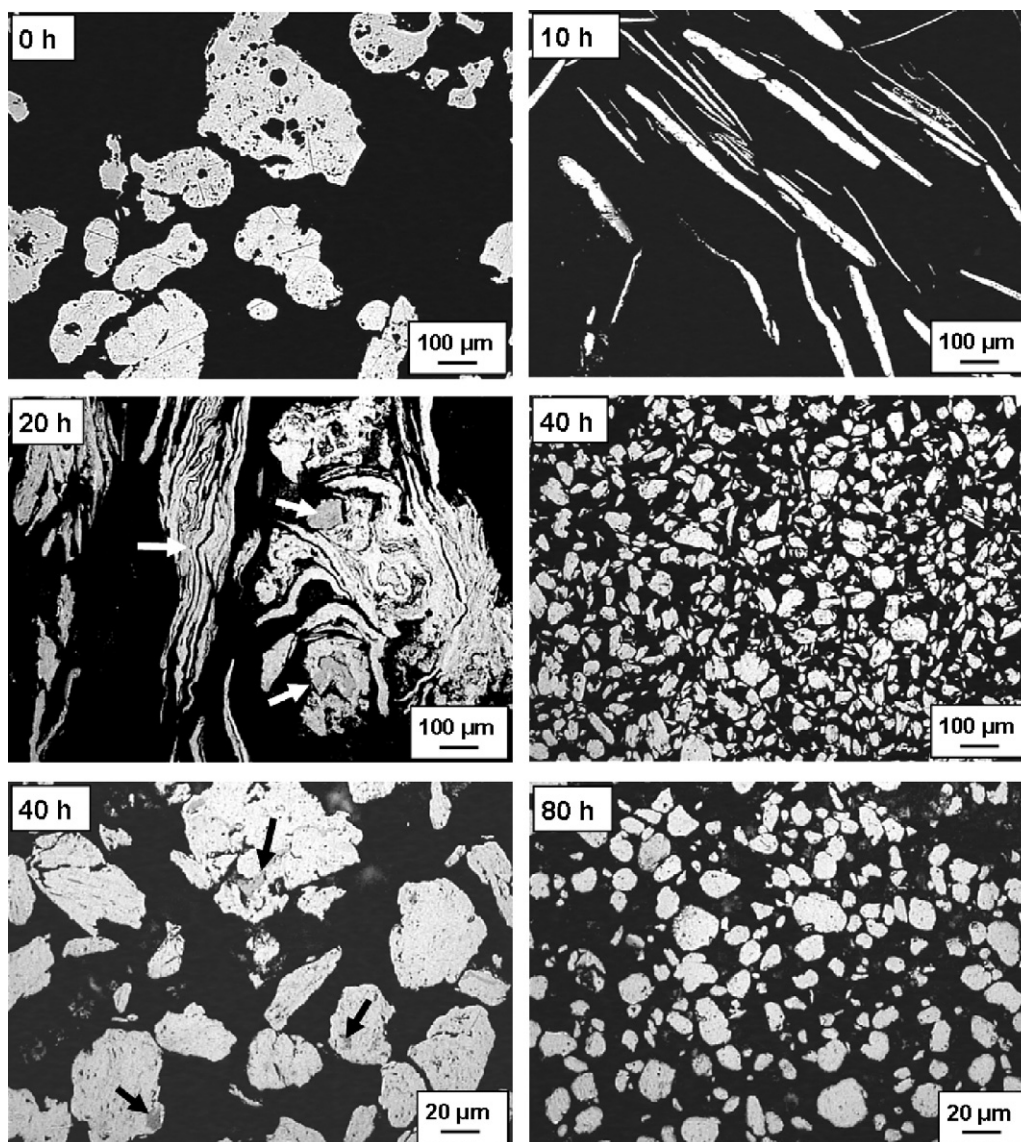


Fig. 2. Changes of morphology of A-2 powder particle during ball milling (light microscopy).

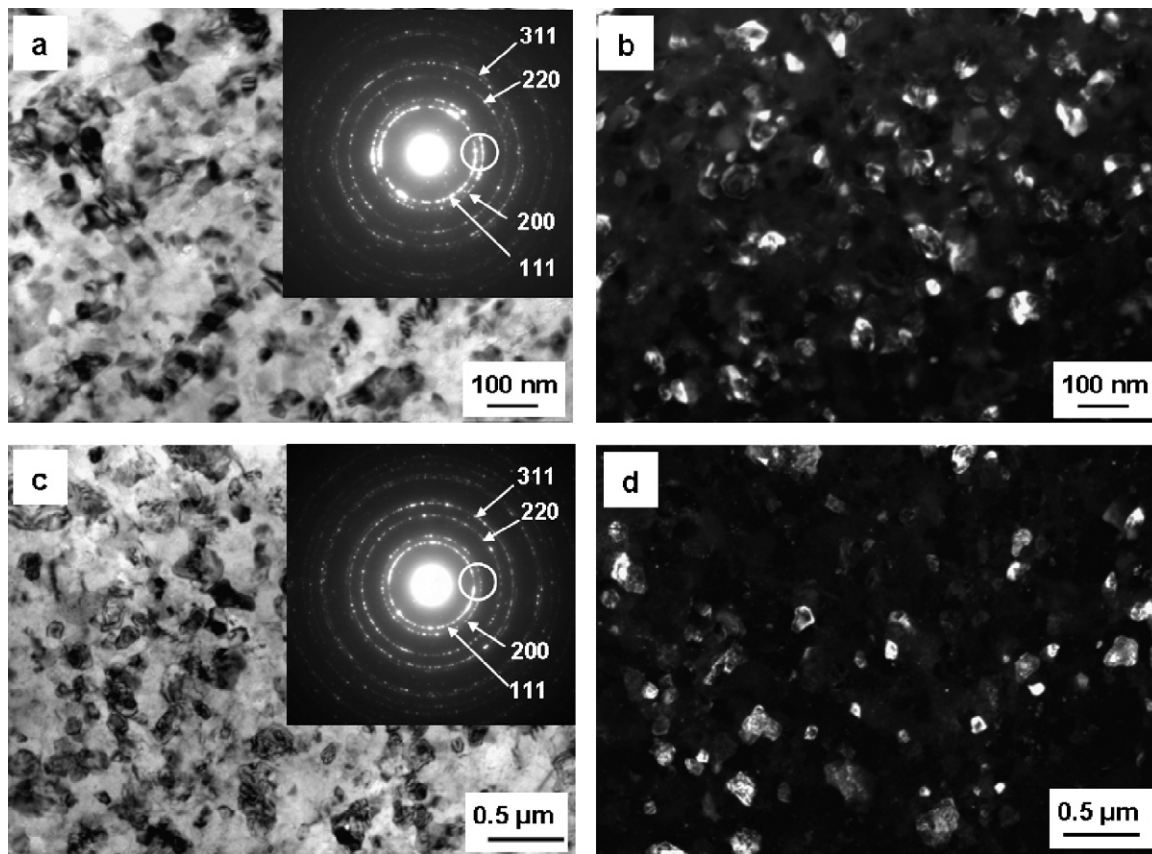


Fig. 3. TEM bright (a, c) and dark (b, d) field images of (a, b) A-0 powder after 80 h of milling and (b, d) compacted A-0 powder; corresponding electron diffraction patterns are inserted (reflections of $\alpha(\text{Al})$ phase are marked). Dark field images were taken using the portion of the 1 1 1 and 0 0 2 diffracted rings of $\alpha(\text{Al})$.

3. Results and discussion

The structure changes of the powders during ball milling process were examined using XRD measurements and light microscopy. Fig. 1 shows, as an example, the sequence of X-ray profiles of A-2 powder blend milled for different time intervals. The reflections of all constituent elements are identified in the initial powder, strong peaks of aluminium and weak of zinc, magnesium, copper and zirconium. At first stage of milling the Mg and Zr lines disappeared, while Zn and Cu lines are present until 40 h of milling. After 20 h of milling a new broad reflection occurred at about 37.8° (marked by arrow in Fig. 1) whose intensity grew as milling proceeded. This peak is not observed in the A-0 powder (without Zr) what means that it represents the Zr containing phase. Patterns for the investigated powder showed a small broadening of $\alpha(\text{Al})$ reflections with increasing milling time, which might be a result of the deformation induced by the milling process and the grain refinement. The position of the $\alpha(\text{Al})$ reflections slightly shifted towards the lower angles and the calculated lattice constant increased up to 4.057 compared to 4.05 for that for initial Al powder due to the dissolution of Zn, Mg and Cu in Al solid solution.

Changes of the morphology of the A-2 powder during milling process are shown in Fig. 2. At the first stage of ball milling, through the collision with the balls, the particles of initial powders underwent deformation and their morphology changed from the initial irregular shape, to flattened one. Then the welding mechanism of flattened particles dominated, leading to mixing of the elemental powder which involves material transfer to obtain homogenous alloy. During that time longer, more equiaxial and harder particles was built which fractured after prolonged milling time. The average size of the powder particles milled 40 h were drastically reduced up

to about 100 μm . As could be seen the particles were not homogeneous and the layers of different composition are visible inside the particles (marked by arrows). This result is consistent with XRD measurements and confirms that particles of initial powders weld together but the mixing of the elements is not finished up to 40 h of milling. Such inhomogeneity inside the particles was not observed after 80 h of milling. Subsequent milling caused the further fragmentation of the powder particles and their estimated mean size after 80 h of milling was about 20 μm .

The nanocrystalline structure was observed in the cross-section of all investigated powders milled for 80 h. In Fig. 3a and b the TEM bright (BF) and dark field (DF) images and selected area diffraction pattern (SADP) of the A-0 powder are shown. Microstructure of grains of size less than 100 nm with rough grain boundaries resulting of deformation during milling process could be seen. The corresponding SADP consists of reflections lying on the rings and only reflections of $\alpha\text{-Al}$ phase were observed and identified. The objective aperture used to take DF image including the portion of the 1 1 1 and 0 0 2 diffracted rings of $\alpha(\text{Al})$ was marked in the SADP.

The zirconium rich particles were observed in the thin foils of the powder A-1 and A-2. Fig. 4a shows a STEM-HAADF image of the A-2 powder after 80 h of milling, in which the Zr-rich particles with a bright contrast are well visible. The size of the Zr-rich particles ranges from a few nanometers up to 200 nm. The chemical micro-analysis performed for the particles lying on the edge of the thin foil (to avoid the influence of the surrounding matrix) showed that they were enriched in Zr and Cu (about 85 wt% of Zr, 14 wt% of Cu and 1 wt% of Al). However, part of the Zr atoms diffused to the Al solid solution which contained up to 0.3 wt% Zr.

Fig. 4b shows the bright-field TEM image and the SADP obtained for the Zr-rich particle. The d_{hkl} spacing's (0.24 nm and 0.28 nm)

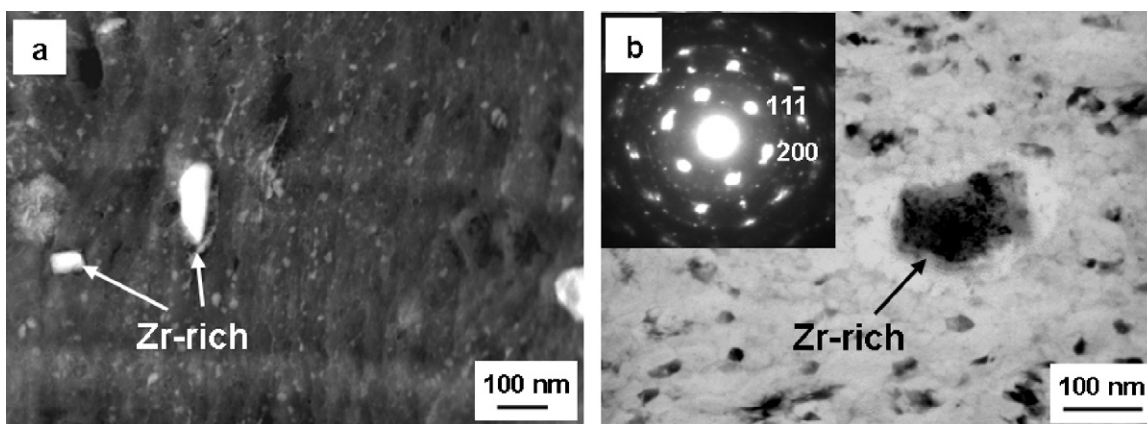


Fig. 4. (a) STEM-HAADF image of the cross-section of the A-2 powder ball milled for 80 h and (b) TEM bright-field image and electron diffraction pattern of A-2 powder milled for 80 h; an fcc phase with zone axis close to $[0\ 1\ 1]$ are identified.

estimated from the diffraction pattern and angles measured between the reflections allowed identifying the Zr-rich compound as fcc phase with a lattice constant 0.48 nm. The proposed fcc phase helped also to explain the additional reflection located at 37.8° in the X-ray diffraction pattern in Fig. 1 which could be fitted to its strongest $(1\ 1\ 1)$ line. A metastable fcc phase with the lattice constant 0.46 nm has been identified in a ball milled powder of pure Zr [13], while it is well known that zirconium exists as the α -(hcp) Zr or β -(bcc) Zr crystal structure below and above 863°C , respectively [14]. A similar fcc phase has also been observed in ball milled mixture of Zr and Al powders [15], Al–Zr–Si alloy [16] and 6061 with Zr addition powder [17].

The hot pressed powders in the form of disc, 20 mm in diameter and 5 mm in height, were of a very good quality, almost without pores and cracks. Fig. 5 shows the X-ray diffraction patterns of the A-0 and A-2 ball milled and hot compacted powders. Besides of the aluminium solid solution lines the reflections identified as MgZn_2 phase are clearly visible for both samples. Like in the ball milled powder, reflection in the position 37.8° could be seen for the Zr containing sample. It means that the zirconium rich particles are stable and did not change during hot compaction process.

The grain size and distribution of the phases determined by TEM observations were similar for A-0, A-1 and A-2 compacted powders. TEM bright- and dark field images as well as SADP obtained for compacted A-0 powder is presented in Fig. 3c and d, where randomly distributed grains of the average size up to about 200 nm could be seen (the mean grain size increases as compared with the

milled powders). Although the MgZn_2 phase was identified in X-ray diffraction pattern (Fig. 5), in the SADP only the α (Al) reflections have been observed.

Distribution of the particles of additional phases was well visible in Z-contrast STEM-HAADF images, while in the conventional TEM images they were difficult to recognize. STEM-HAADF image of the A-0 compacted powder presented in Fig. 6 shows small particles of MgZn_2 phase inside the grains. Occasionally larger particles enriched in Fe, Cu and Zn were also observed.

The microhardness as well as the compression tests results for A-0, A-1 and A-2 compacted powders are presented in Table 1. The Vickers microhardness measurements were performed on the cross section of the compacted powders. Hardness was determined by the Oliver and Pharr method [18] and the mean value of the microhardness calculated from 10 measurements are presented. The microhardness about 195 HV characterizes all samples and is consistent with the results of compression tests. The ultimate compression strengths is about 650 MPa for A-0 and A-2 samples and slightly lower (611 MPa) for A-1 sample. The Young's modulus is about 50 GPa for A-0 and A-1 samples and about 52 GPa for A-2. It may be noted that the differences between the properties of investigated samples are minimal. Thus, it can be concluded that addition of zirconium had no influence on the strength of the compacted powders. In Fig. 7 the compression curve of the hot pressed A-2 powder is shown as an example.

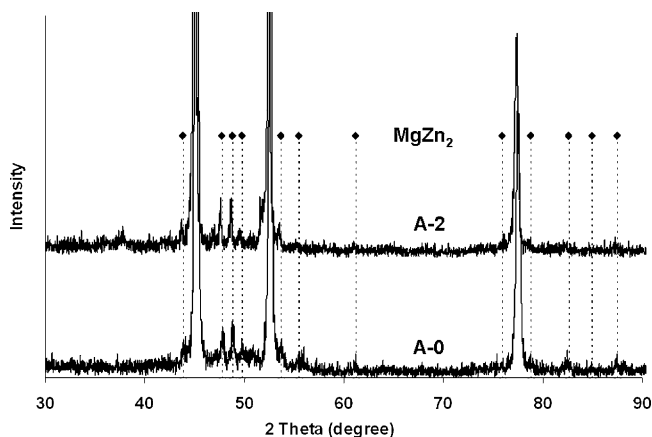


Fig. 5. X-ray patterns of A-0 and A-2 powders milled for 80 h and hot compacted.

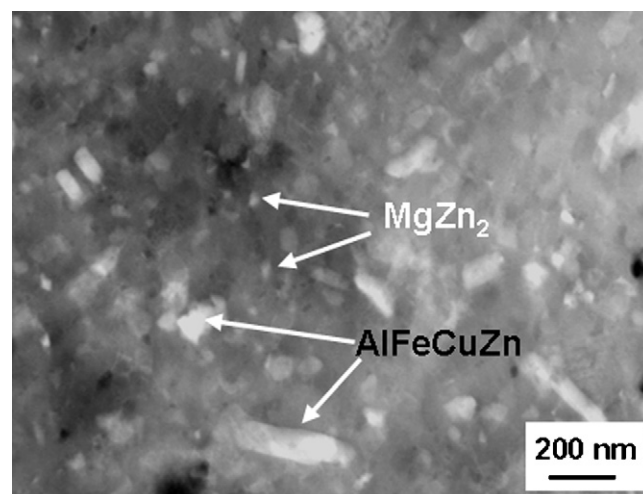


Fig. 6. STEM-HAADF images of the A-0 compacted powder.

Table 1
Vickers microhardness [0.2 N] and compression tests results for A-0, A-1 and A-2 compacted powders.

Material	Microhardness [HV 0.2 N]	Ultimate compression strength [MPa]	Young's modulus [GPa]
A-0	194 ± 8	643	50.1
A-1	195 ± 8	611	50.2
A-2	192 ± 9	658	52.3

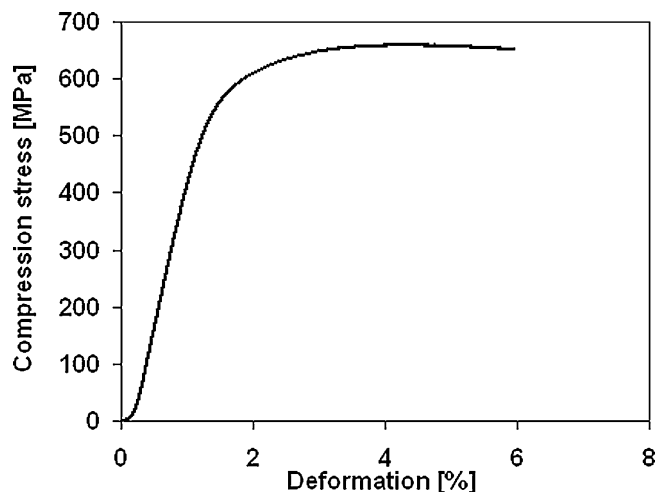


Fig. 7. Compression curve of the hot pressed A-2 powder.

4. Conclusions

- Ball milling of the elemental powder of the composition Al–12 wt% Zn–3 wt% Mg–1.5 wt% Cu with addition of 1 and 2 wt% Zr leads to homogenous mixture of nanocrystalline aluminium solid solution of grain size about 100 nm after 80 h of milling. The Zr and Cu rich particles of the fcc structure were identified in Zr containing powders.
- Hot pressing in vacuum allows to obtain good quality disc without pores and cracks contained regular grains of about 200 nm with well defined grain boundaries and reduced, compared to milled powder, dislocation density. The MgZn₂ phase was identified in the compacted powder located inside the grains.
- The microhardness about 195 HV (0.2 N) and the ultimate compression strengths in the range 611–658 MPa were characterized all investigated samples. Addition of zirconium had no influence on the strength of the compacted powders.

Acknowledgement

This work was financially supported by the Polish Ministry of Science and High Education (Research Project 4485/B/T02/2008/34).

References

- [1] I.J. Palmear, *Light Alloys: From Traditional Alloys to Nanocrystals*, Elsevier, 2006.
- [2] T.S. Srivatsan, S. Sriram, D. Veeraraghavan, V.K. Vasudevan, *J. Mater. Sci.* 32 (1997) 2883–2894.
- [3] I.N. Fridlyander, *Met. Sci. Heat Treat.* 45 (2003) 341–343.
- [4] Y.L. Wu, F.H. Froes, A. Alvarez, C.G. Li, J. Liu, *Mater. Des.* 18 (1997) 211–215.
- [5] H. Adachi, K. Osamura, S. Ochiai, J. Kusui, K. Yokoe, *Scripta Mater.* 44 (2001) 1489–1492.
- [6] M.M. Sharma, M.F. Amateau, T.J. Eden, *Acta Mater.* 53 (2005) 2919–2924.
- [7] J. Kusui, K. Fujii, K. Yokoe, T. Yokote, K. Osamura, O. Kubota, H. Okuda, *Mater. Sci. Forum* 217–222 (1996) 1823–1828.
- [8] K.L. Kendig, D.B. Miracle, *Acta Mater.* 50 (2002) 4165–4175.
- [9] C. Suryanarayana, *Prog. Mater. Sci.* 46 (2001) 1–184.
- [10] A.V. Sameljuk, O.D. Neikov, A.V. Krajnikov, Yu.V. Milman, G.E. Thompson, X. Zhou, *Corros. Sci.* 49 (2007) 276–286.
- [11] J.D. Robson, P.B. Prangnell, *Acta Mater.* 49 (2001) 599–606.
- [12] H. Adachi, K. Osamura, J. Kusui, S. Okaniwa, *Mater. Sci. Forum* 519–521 (2006) 1479–1484.
- [13] I. Manna, P.P. Chattopadhyay, F. Banhart, H.-J. Fecht, *Appl. Phys. Lett.* 81 (2002) 4136–4138.
- [14] T. Massalski (Ed.), *Binary Alloy Phase Diagrams*, vol. 1, ASM-International, USA, 1990, pp. 241–243.
- [15] H.J. Fecht, G. Han, Z. Fu, W.L. Johnson, *J. Appl. Phys.* 67 (1990) 1744–1748.
- [16] I. Manna, P.P. Chattopadhyay, F. Banhart, H.-J. Fecht, *Z. Metallkd.* 94 (2003) 835–841.
- [17] L. Lityńska-Dobrzyńska, J. Dutkiewicz, W. Maziarz, Ł. Rogal, *J. Microsc.* 237 (2010) 506–510.
- [18] W.C. Oliver, G.M. Pharr, *J. Mater. Res.* 7 (1992) 1564–1583.